Chapter 6

Exciton quenching in polymer light-emitting diodes

Summary

The quenching of excitons at the metallic cathode of a polymer light-emitting diode (PLED) has been investigated by time-resolved photoluminescence. The decay of the luminescence is analyzed including both nonradiative energy transfer to the metallic cathode and exciton diffusion. Incorporation of the resulting exciton density profiles into a PLED device model consistently describes the reduction of the quantum efficiency at low bias voltage.

6.1 Introduction

Polymer light-emitting diodes (PLEDs) [1] are considered to be attractive candidates for lighting and large-area display applications [2]. It has been recognized that charge transport is one of the key ingredients for the PLED performance [3]. For derivatives of poly(*p*-phenylene vinylene) (PPV) it has been obtained that the electron conduction is significantly smaller than the hole conduction, which is attributed to the presence of traps [4] or lower electron mobility [5]. For PLEDs, in which both electrons and holes are injected, the different conduction of electrons and holes is directly responsible for the distribution of the exciton generation in the polymer layer. Model calculations on single layer PLEDs demonstrated that at low voltages most of the excitons are formed close to the cathode, due to the reduced electron transport in PPVs [6].

The competition between radiative and nonradiative excitonic processes in conjugated polymers is another important issue that governs the conversion efficiency (CE), defined as photon/charge carrier, of a PLED. Singlet/triplet exciton formation branching and nonradiative quenching of excitons via defects also limit the CE of a PLED [7, 8]. Furthermore, the presence of a metallic cathode opens up an additional exciton loss channel via nonradiative energy transfer to the metal. Thus, confinement of the exciton generation profile to the metallic cathode, where excitons are effectively quenched, is expected to strongly reduce the PLED efficiency at low voltages. For higher voltages, the exciton concentration is more uniformly distributed throughout the PLED device. The increase of CE with voltage could be fitted by assuming a quenching region of typically 10 nm for single-layer dialkoxy-PPV light-emitting diodes [6]. From photoluminescence (PL) experiments, a typical width of the quenching region of 20 nm has been obtained for cyano derivatives of PPV [9].

Although the 10 nm estimation from the PLED device model is in reasonable agreement with the luminescence data, it should be noted that it is based on a number of assumptions: First, in the model, the quenching of excitons is approximated by simply ignoring all excitons that are generated within the first 10 nm of the cathode when calculating the total light output. Outside the 10 nm region the quenching is zero, thus the quenching process is approximated by a steplike profile. However, nonradiative energy transfer toward a metallic cathode is known to be strongly distance dependent [10]. Furthermore, the energy transfer will lead to a strong gradient in the exciton population, and resulting vacancies will be refilled by exciton diffusion. It is demonstrated that the effective quenching region of 15 nm can be decomposed in an energy transfer range of 7.5 nm and an exciton diffusion length L_D of 6 nm [11]. In the present study, the quenching of excitons at the Ba/Al cathode of a NRS-PPV based PLED is investigated using time-resolved PL measurements. The extracted parameters describing exciton diffusion and quenching are subsequently incorporated into a PLED device model [6] that is based on experimental results of charge transport and bimolecular recombination. This combined optical and electrical characterization consistently explains the voltage dependence of the conversion efficiency of this PPV-based PLED.

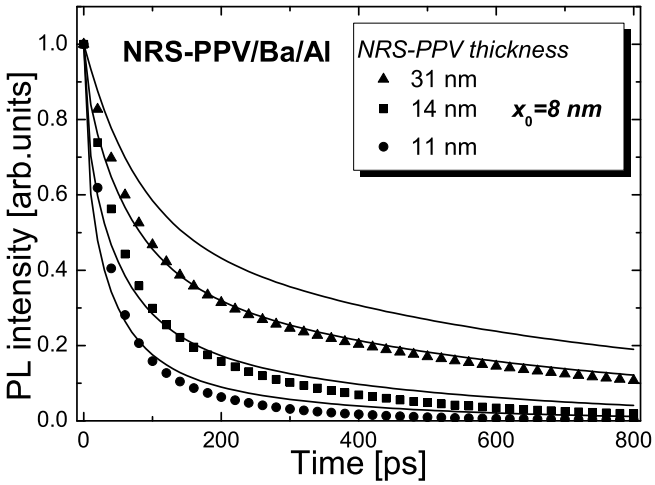

Figure 6.1: Deconvoluted and normalized PL decay curves in polymer/metal structures with variable polymer film thickness (symbols). Lines are fits of these data to Eq. (6.1) with $x_0 = 8$ nm and $D = 3 \times 10^{-4}$ cm^2/s.

6.2 Optical characterization of the quenching dynamics

As a first step, we investigate the modification of the time-resolved PL of NRS-PPV due to the presence of a Ba/Al cathode. NRS-PPV was spin-coated from toluene solution on a glass substrate; the film thickness was varied by changing the spin speed. Layers of barium (5 nm) and aluminum (100 nm) were subsequently thermally evaporated on top, representing a typical PLED cathode. The decay curves of the PL in these heterostructures are shown in Fig. 1, together with the PL decay curve of the neat polymer. Reduction of the polymer film thickness results in a faster decay of the exciton population. Frequency-doubled laser pulses (FWHM=200 fs, 400 nm) were used for excitation of the polymer luminescence; the emission was registered at its maximum, 580 nm. In Fig. 6.1, the PL decay curves are shown after deconvolution with the instrument response function (FWHM=30 ps) and normalization.

In order to quantify the exciton quenching mechanism, the time-resolved PL data (Fig. 6.1) were modeled with a modification of Eq. (5.9) assuming direct polymer-metal contact ($d = 0$) [11]

$$\frac{\partial n(x,t)}{\partial t} = D\frac{\partial^2 n(x,t)}{\partial x^2} - \frac{n(x,t)}{\tau_\infty(t)}\left(1 + \frac{{x_0}^3}{x^3}\right) + g(x,t). \tag{6.1}$$

Here, the second term accounts for radiative and nonradiative exciton decay in the polymer (lifetime τ_∞), further enhanced by nonradiative exciton energy transfer to the metal, described by the inverse cubic distance dependence.

Numerical modeling of the time-resolved PL in NRS-PPV/Ba/Al structures

(Fig. 6.1) with Eq. (6.1) was carried out using the exciton diffusion constant D, as determined in our previous studies [12]. The energy-transfer range x_0 is the only parameter to simultaneously fit all PL decay curves measured for different thickness of the polymer films. A value of 8 nm is obtained for the NRS-PPV/Al/Ba hetrostructure, being nearly equal to the 7.5 nm previously found for an Al electrode [11]. With D and x_0 known, the steady-state exciton density profile can be calculated, taking into account the quenching at the Ba/Al cathode.

6.3 Voltage dependence of the PLED conversion efficiency

In order to demonstrate the implications of these findings for the device operation of a NRS-PPV-based PLED, we have to take into account the positional dependence of the exciton generation rate $g(x)$. In a PLED, the spatial generation of excitons is governed by the charge transport properties of the injected electrons and holes. In order to calculate the distribution of free electrons $n(x)$ and holes $p(x)$ inside the PLED, we make use of a standard device model that has been explained in detail previously [6]. The hole mobility has been derived from space-charge-limited current-voltage characteristics; a zero-field mobility of 1.5×10^{-12} m^2/Vs is used in this model [13, 14]. Electron and hole mobilities are assumed to be equal, and the electron transport is strongly limited by an exponential distribution of trapping sites, characterized by a density of traps $N_t = 8 \times 10^{23}$ m^{-3} and a trap temperature $T_t = 1100$ K [4, 15]. The bimolecular recombination (rate B) between free electrons and holes is of the Langevin type. As a result the profile $g(x)$ of exciton generation in the PLED is given by $Bn(x)p(x)$. In Fig. 6.2, $n(x)$ and $p(x)$ are shown for a PLED based on a 124 nm thick NRS-PPV film, together with the exciton generation profile $Bn(x)p(x)$ for a bias voltage of 2.4 V.

As a next step, this exciton generation profile is incorporated into Eq. (6.1), together with D and x_0 as determined from the luminescence decay curves. The steady-state exciton distribution in the PLED is calculated by setting $\partial n(x,t)/\partial t = 0$. Figure 3 shows the calculated profiles of the exciton density. For comparison, the dotted profile represents the previous model that simply ignores the radiative decay of the excitons within the width L_q at the cathode, in order to take exciton quenching into account [6]. In that model L_q has been used as a fit parameter to simulate the voltage dependence of the PLED conversion efficiency. The solid line (Fig. 6.3) shows the numerical steady-state solution of Eq. (6.1), where the exciton generation profile $Bn(x)p(x)$ from Fig. 6.2 is taken to represent the last term. The exciton density peaks at 13 nm away from the cathode at 2.4 V, and then gradually decreases further away from the cathode.

In Fig. 6.4, the normalized experimental CE of a NRS-PPV-based PLED with a polymer film thickness of 124 nm and a Ba/Al top contact is shown. Due to the strong enhancement of the electron transport with increasing voltage, the exciton generation profile shifts away from the quenching zone at the cathode, leading to an improved CE. With the exciton profiles and the resulting amount of quenching known at any

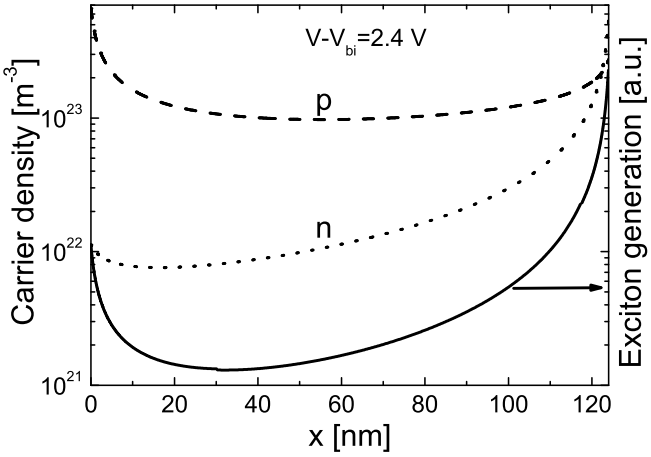

Figure 6.2: Hole (p, dashed curve) and electron (n, dotted curve) density distribution in the cross-section of the device simulated with a PLED model. Also shown is the exciton generation profile (solid curve) assuming Langevin recombination of the charge carriers.

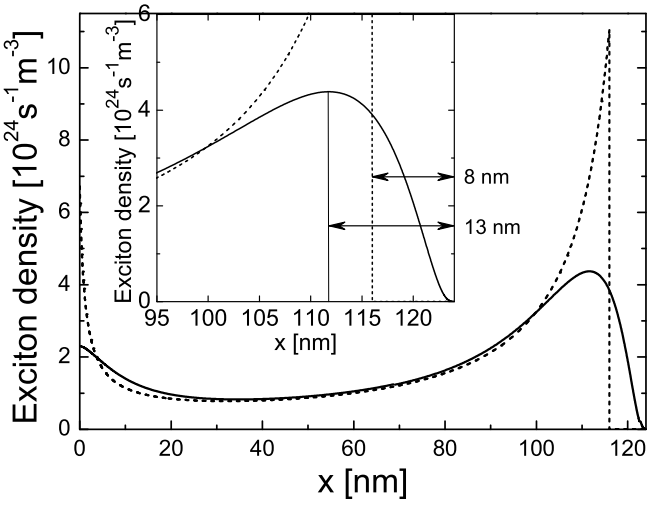

Figure 6.3: Exciton density profile (solid curve) simulated for a bias voltage of 2.4 V. Exciton profile (as implied in Ref. [6]) is shown for comparison (dashed curve).

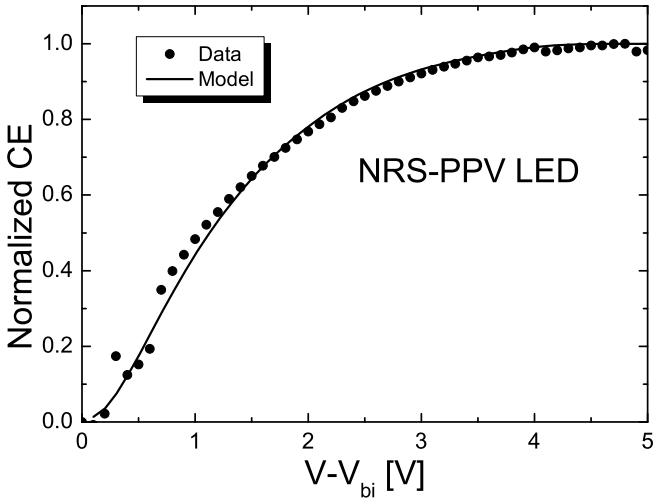

Figure 6.4: Normalized efficiency CE vs voltage for ITO/NRS-PPV/Ba/Al LED form experiment (•) and model (line). Exciton quenching parameters used are obtained in from optical experiments.

applied voltage, the increase of CE with voltage can be now calculated without any fit parameter. The two parameters that govern the spatial distribution of excitons, D and x_0, have both been independently determined from time-resolved luminescence measurements (Fig. 6.1). As shown in Fig. 6.4 the calculated CE is in good agreement with the experimental results, showing that our model quantitatively accounts for the exciton quenching at the cathode of the PLED.

6.4 Conclusions

In conclusion, we have studied the quenching of excitons at the cathode of a PLED and its relevance to the device performance. The diffusion of excitons and nonradiative energy transfer to the cathode were characterized by means of time-resolved PL. The results of these optical studies were implemented in a PLED device model and the exciton density profiles at any applied voltage are calculated. This combined optical and electrical characterization leads to a quantitative description of the voltage dependence of the conversion efficiency of a NRS-PPV based PLED.

Bibliography

[1] J. H. Burroughes, D. D. C. Bradley, A. R. Brown, R. N. Marks, K. Mackay, R. H. Friend, P. L. Burns, and A. B. Holmes, Nature (London) **347**, 539 (1990).

[2] H. Kobayashi, S. Kanbe, S. Seki, H. Kigchi, M. Kimura, I. Yudasaka, S. Miyashita, T. Shimoda, C. R. Towns, J. H. Burroughes, and R.H.Friend, Synth. Met. **111-112**, 125 (2000).

[3] D. D. C. Bradley, A. R. Brown, P. L. Burn, R. H. Friend, A. B. Holmes, and A. Kraft, *Electronic Properties of Polymers, Solid State Sciences* (Springer, Heidelberg, 1992), Vol. 107, p. 304.

[4] P. W. M. Blom, M. J. M. de Jong, and J. J. M. Vleggaar, Appl. Phys. Lett. **68**, 3308 (1996).

[5] L. Bozano, S. A. Carter, J. C. Scott, G. G. Malliaras, and P. J. Brock, Appl. Phys. Lett. **74**, 1132 (1999).

[6] P. W. M. Blom and M. C. J. M. Vissenberg, Mater. Sci. Eng., R. **27**, 53 (2000).

[7] R. H. Friend, R. W. Gymer, A. B. Holmes, J. H. Burroughes, R. N. Marks, C. Taliani, D. D. C. Bradley, D. A. Dos Santos, J. L. Bredas, M. Logdlund, and W. R. Salaneck, Nature (London) **397**, 121 (1999).

[8] J. S. Wilson, A. S. Dhoot, A. J. A. B. Seeley, M. S. Khan, A. Kohler, and R.H.Friend, Nature (London) **413**, 828 (2001).

[9] H. Becker, S. E. Burns, and R. H. Friend, Phys. Rev. B **56**, 1893 (1997).

[10] R. R. Chance, A. Prock, and R. Silbey, J. Chem. Phys. **62**, 2245 (1975).

[11] D. E. Markov and P. W. M. Blom, Phys. Rev. B **72**, 161401(R) (2005).

[12] D. E. Markov, J. C. Hummelen, P. W. M. Blom, and A. B. Sieval, Phys. Rev. B **72**, 045216 (2005).

[13] C. Tanase, P. W. M. Blom, D. M. de Leeuw, and E. J. Meijer, Phys. Status Solidi A **201**, 1236 (2004).

[14] C. Tanase, J. Wildeman, P. W. M. Blom, M. E. Mena Benito, D. M. de Leeuw, A. J. J. M. van Breemen, P. T. Herwig, C. H. T. Chlon, J. Sweelssen, and H. F. M. Schoo, J. Appl. Phys. **97**, 123703 (2005).

[15] M. M. Mandoc, B. de Boer, and P. W. M. Blom (unpublished).